



## Research on SiC/C and SiC/Cu FGM for Plasma Facing Materials

**Chang-Chun GE**

Institute of Nuclear Materials,  
University of Science and Technology Beijing (INM,  
USTB), P.R. China

## **Contributors**

**Chang-Chun GE<sup>1, 4</sup>, Shuang-Quan GUO<sup>1, 4</sup>, Hong-Yan GUO<sup>1, 4</sup>,  
Xiao-Feng ZHANG<sup>1, 5</sup>, Qing-Zhi YAN<sup>1</sup>, Xiang LIU<sup>2</sup>, Ming-Xu WANG<sup>2</sup>  
Li-Ping GUO<sup>3</sup>**

**<sup>1</sup> Institute of Nuclear Materials, University of Science and Technology  
Beijing (INM, USTB), Beijing 100083, P.R. China;**

**<sup>2</sup>South-Western Institute of Physics**

**<sup>3</sup>Key Laboratory of Artificial Micro- and Nano-  
structures of Ministry of Education and School of Physics and Tech  
nology, Wuhan University, Wuhan 430072, P.R. China;**

**<sup>4</sup>School of Materials Science & Engineering, Southwest Jiaotong  
University, Chengdu 610031, P. R. China;**

**<sup>5</sup> School of Materials Science & Engineering, Jingdezhen Ceramic  
Institute, Jingdezhen, 333001**

# **contents**

**1 Introduction**

**2 Experimental procedure**

**3 Results and discussion**

**4 Conclusion**

# 1. Introduction

Plasma facing materials and components (PFM/PFC) not only play the key role but also are the greatest technical difficult part in magnetic constraint fusion. W-based PFM is now looked as the most perspective candidate for future fusion reactors. But it has several disadvantages: high ductile-to-brittle transition temperature (DBTT); low recrystallization temperature, neutron irradiation brittleness under very low dose. Hence when we put emphasis on research of W-based PFM, we should not neglect to research on other materials for PFM. Silicon carbide (SiC) as a low atomic number (Z) compound has a series of advantages for use in fusion reactors, such as low contamination to plasma, good high-temperature properties, high corrosion resistance, low density, and especially its environmentally benign property for low-induced radioactivity after neutron irradiation.

**The FGM design idea for making SiC/C and SiC/Cu plasma-facing FGM was proposed by the author and research on design and fabrication of SiC/C and SiC/Cu plasma-facing FGM was conducted in LSCPM since 1997 with the aim to combine the excellent high temperature properties, low chemical sputtering, high erosion resistance, and low activation after irradiation of SiC with the high thermal conductivity of graphite and copper, to reduce the thermal stress caused by the mismatch of thermal expansion coefficients on the interfaces and to prevent the cracks and failure under serious plasma erosion conditions.**

**In this study, the design and fabrication and plasma-relevant characteristics of SiC/C FGM and SiC/Cu FGM were investigated. Microstructure analysis, thermal shock resistance, chemical sputtering and thermal desorption performances of SiC/C and SiC/Cu FGMs were conducted. In addition, the effect of 700°C implantation of helium in SiC was preliminarily studied with the heavy ion research facility in Institute of Modern Physics, Chinese Academy of Sciences, Lanzhou (HIRFL) and accelerator in the School of Physics and Technology of Wuhan University. The possibility of using SiC/C FGM and SiC/Cu both as future first wall materials is discussed.**

## 2. Experimental procedure

The design of compositional distribution in the graded layers of the FGM:  $f = (x/d)^p$ , where  $f$  is the volume fraction,  $x$  the relative distance from the surface,  $d$  the thickness of the FGM layer, and  $p$  the compositional distribution factor. In FGMs processing, it is very important to optimize  $p$  values for relaxing thermal residual stress due to the mismatch of CTEs. SiC/C and SiC/Cu FGMs with different  $p$  values were designed and optimized.

SiC/Cu FGMs were fabricated by resistance sintering under ultra-high pressure (RSUHP). SiC/C FGM was made with powder stacking-hot pressing.

## 2. Results and discussion

### *3.1 Microstructure of SiC/C and SiC/Cu FGM*

**Fig. 1-2 shows the cross sectional back-scattered image of SiC/C FGM with four layers. SiC particles are gray, while C shows columnar structure in black. Remarkable compositional changes are evident, which reflects no significant elemental migration during material processing as shown in Fig. 1-2(a). The line scanning EDS spectra of Si indicate that the content of SiC is gradually changed from the SiC side to the C side of the SiC/C FGM except for the interfaces between neighboring graded layers. Fig. 1-2(b) depicts the morphology of the interface between graded layer (20% C + 80% SiC) and layer (40% C + 60%SiC). It is obvious that SiC and C have been sintered and bonded well together, no macro cracks or pores were found in SiC/C FGM. The composition between neighboring graded layers is gradually changed so that the similar morphology is shown in other interfaces of all SiC/C FGM samples.**

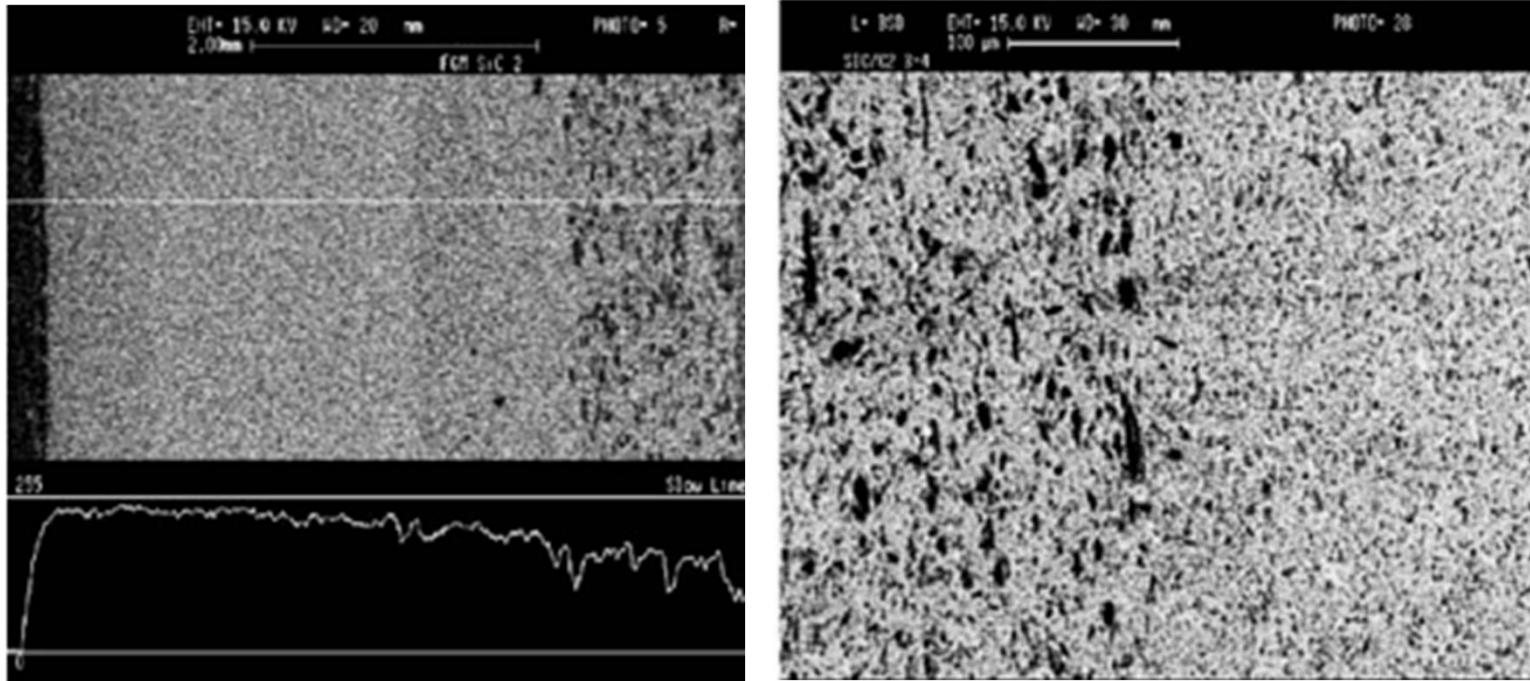


Fig. 1-2 Microstructure of SiC/C FGM: (a) micrograph; (b) interface.

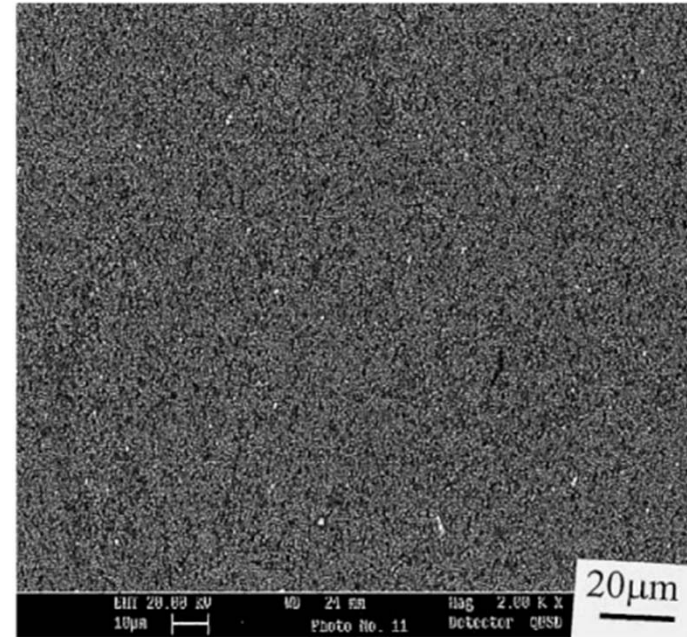
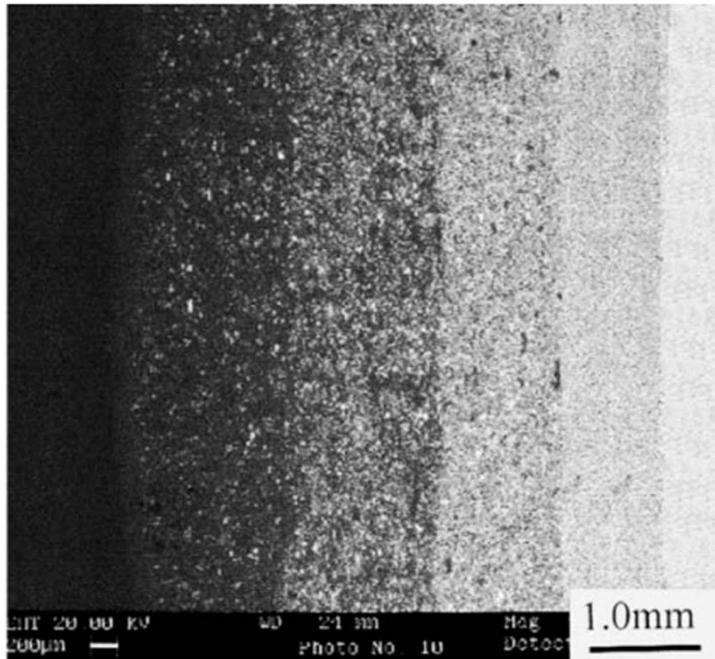


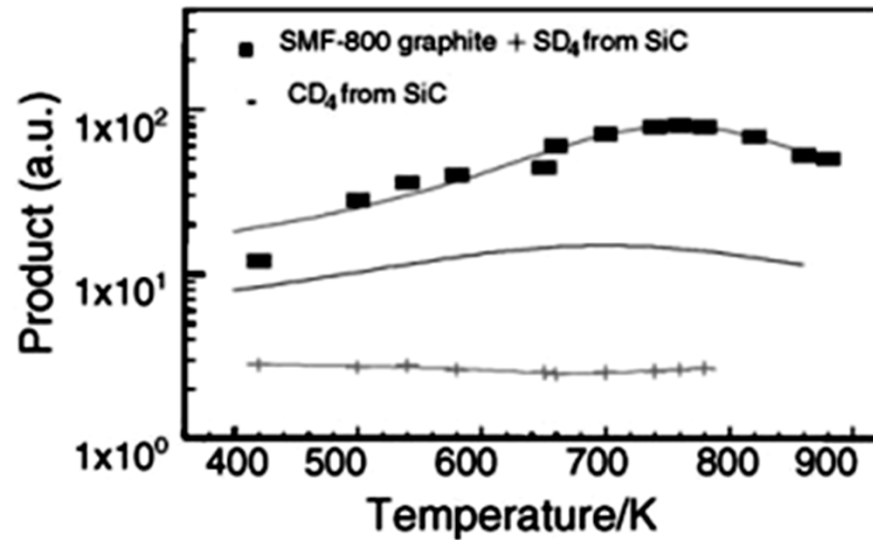
Fig.3-4 (a) SEM of overall six-layered SiC/Cu FGM with  $p = 1.0$  after heat treatment (Cu contents are 0, 20, 40, 60, 80, 100vol. %, respectively). (b) pure ceramic layer of SiC/Cu FGM.

**Fig. 3-4(a) presents a back-scattered image of the overall six-layered SiC/Cu FGM. From that pronounced compositional changes were demonstrated, which reflects no macro elemental migration during rapid sintering under ultra-high pressure and subsequent short duration of heat treatment. Fig.3-4(b) depicts microstructure of pure SiC ceramics (the top layer) of SiC/Cu FGM, it is obvious that SiC has been sintered and bonded well together.**

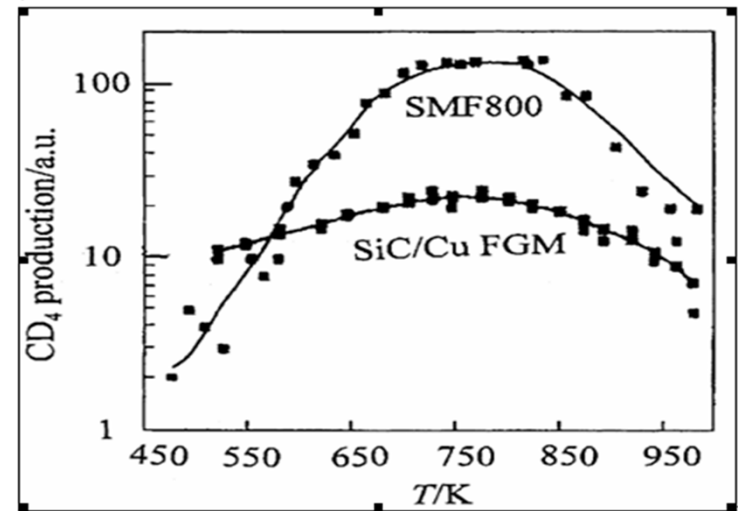
### ***3.2. Chemical sputtering and thermal desorption performances***

The chemical sputtering performance of SiC/C and SiC/Cu FGMs after heat treatment was conducted in LAS-2000 apparatus. The sputtering products were measured under irradiation of 3 keV,  $4.6 \times 10^{15} \text{ s}^{-1} \text{ cm}^{-2}$  and the change of ratio  $\text{SiD}_4^+ / \text{CD}_4^+$  with temperature was recorded by mass-spectrometry.

As shown in Fig. 5(a), in comparison with graphite SMF-800, SiC/C FGM shows lower  $\text{SiD}_4/\text{CD}_4$  yield. The  $\text{SiD}_4$  and  $\text{CD}_4$  product at 500 K of SiC/C FGM is 2.8 and 10 a.u., respectively. The total  $\text{SiD}_4 + \text{CD}_4$  product of SiC/C FGM at 500 K is 47% of that of graphite SMF-800, while at 700 K is 22% of that of graphite. At the high temperature, the total  $\text{SiD}_4 + \text{CD}_4$  product of SiC/C FGM is 20–30% of that of graphite, so the SiC/C FGM has better erosion resistant property than graphite SMF-800. In Fig. 5 (b) SiC/Cu FGM shows much lower  $\text{CD}_4$  production than graphite SMF800, the peak value of  $\text{CD}_4$  production, which reached at 750 K, is about 15% of that graphite SMF800, and the temperature of  $\text{CD}_4$  peak value shifts to a lower 30 K.



(a)



(b)

Fig.5. (a) The chemical sputtering yields of SiC/C FGM and graphite SMF-800, (b) Temperature dependences of  $CD_4$  products under 3keV,  $4.6 \times 10^{15} D + s^{-1} cm^{-2}$  irradiation.

**Fig. 6 shows the TDS data of SiC/C FGM and graphite SMF-800. D<sub>2</sub> is the major deuterium species out-gassed from the samples; the yields of D<sub>2</sub> of SiC/C FGM and graphite SMF-800 are similar. But the major difference is the amount of CD<sub>4</sub> molecules outgassed from the sample. The yields of CD<sub>4</sub> of SiC/C FGM are obviously lower than that of graphite SMF-800 at least one order of magnitude lower, and the yield of SiD<sub>4</sub> is lower than that of CD<sub>4</sub> by SiC/C FGM at least one order of magnitude. The experimental results of Fig.6 indicate that SiC/C FGM has better hydrogen isotope retention behavior after plasma exposure than graphite SMF-800.**

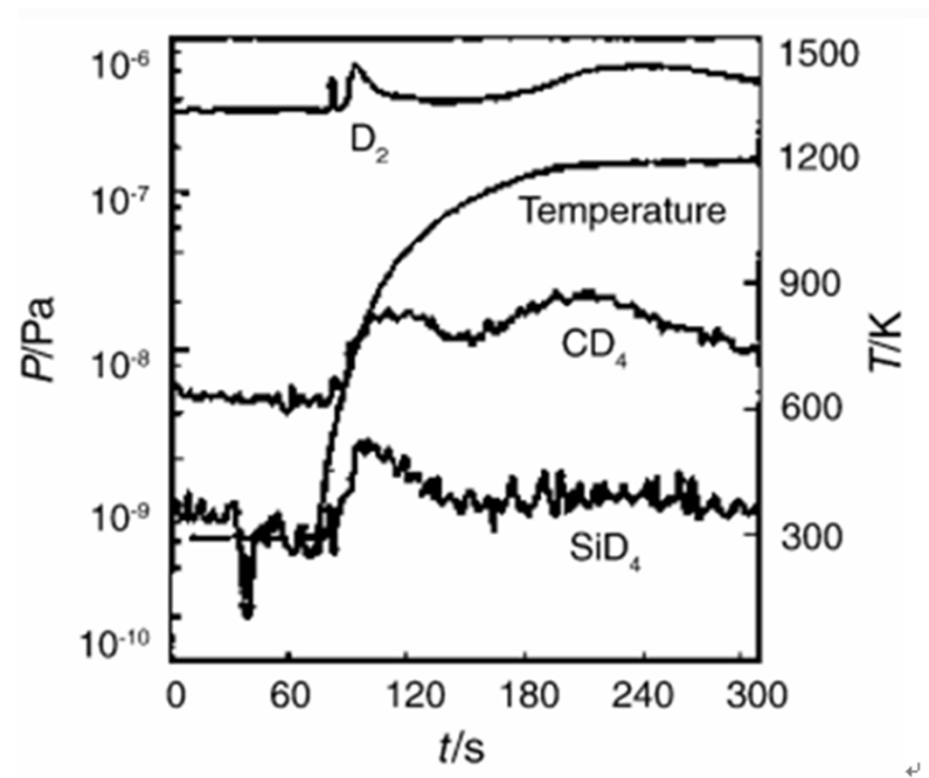
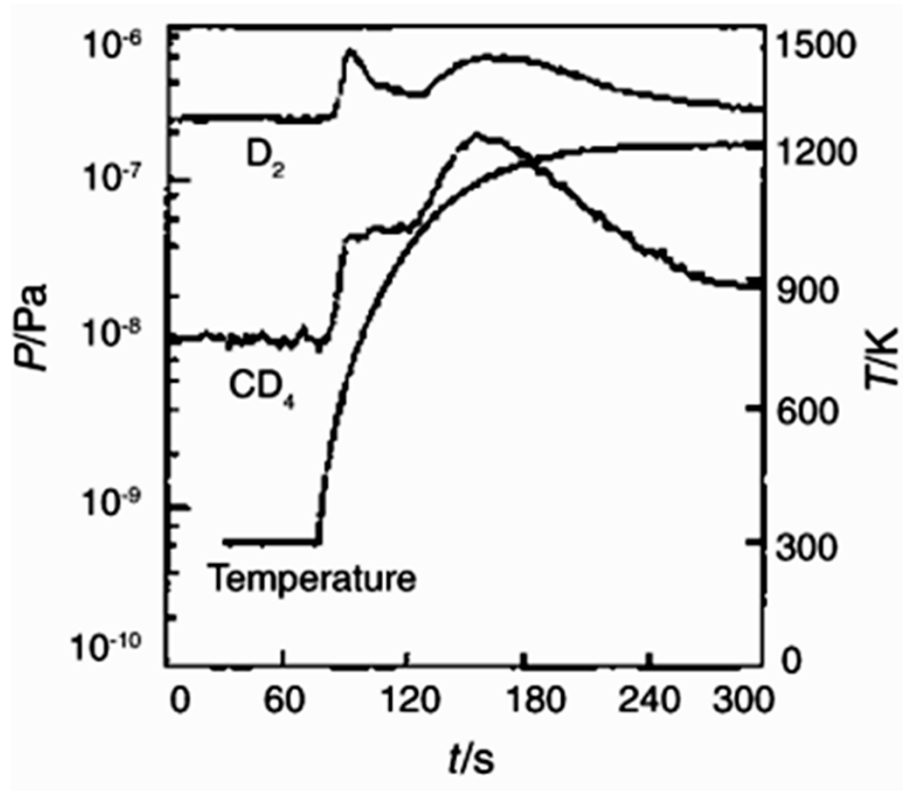


Fig. 6 The thermal desorption spectra of SiC/C FGM and graphite SMF-800.

**In Figs.7 the results of the TDS data of SiC/Cu FGM together with the curve of temperature rise were drafted in the figures. The CD<sub>4</sub> production of SiC is obviously lower than that of graphite, approximately 10% of that graphite SMF800 and the SiD<sub>4</sub> production is lower than that of CD<sub>4</sub> by at least one order less.**

**It can be concluded from above-mentioned results that SiC has higher chemical sputtering resistance under plasma irradiation than that of nuclear graphite SMF800, and its lower gas desorption compared with nuclear graphite also means lower deuterium retention in D–T reaction and therefore SiC will be beneficial to the circulation of fuel deuterium in fusion device.**

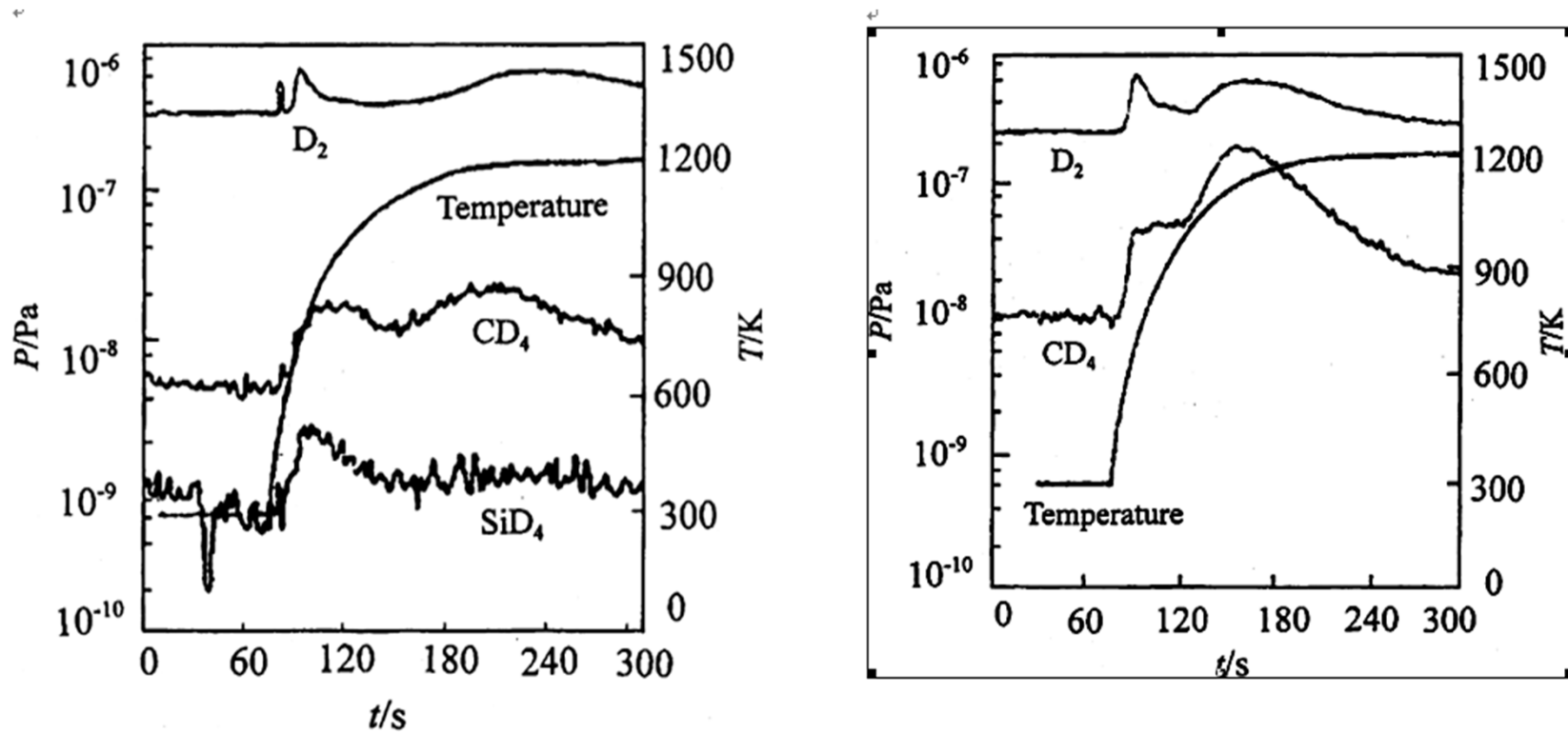
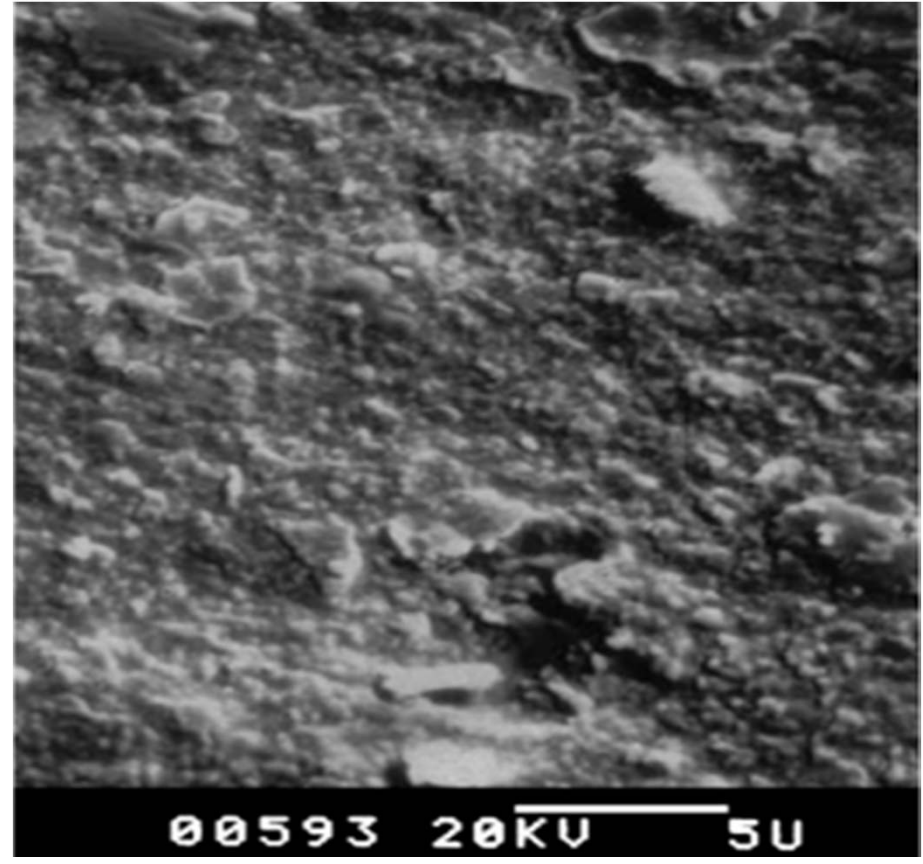
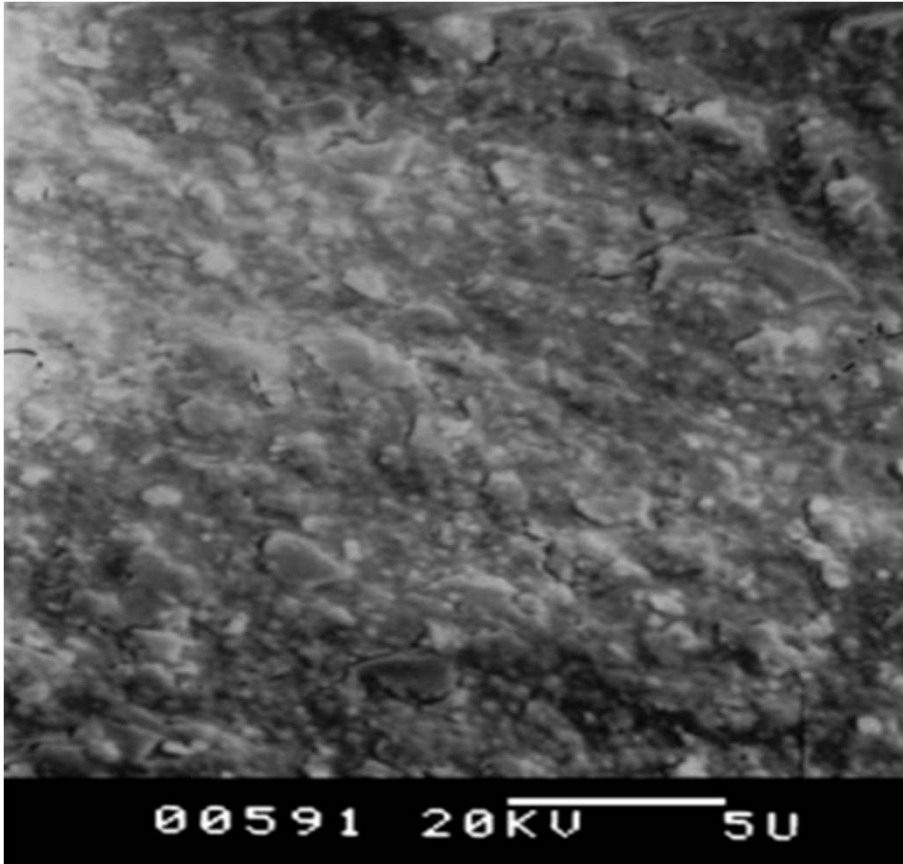


Fig.7. The thermal desorption spectra of SiC/Cu FGM and graphite SMF-800

### ***3.3. Physical sputtering in Tokamak apparatus***

**In order to measure the comprehensive resistance to plasma erosion at high temperature, 11-layered SiC/C and SiC/Cu FGMs were put into a Tokamak apparatus and eroded by the severe plasma irradiation for 66 pulses. The irradiation parameters of HL-1M apparatus were: perpendicular magnetic field: 2 T; loop electric current: 120–200 kA; average pulse time of plasma: 1.2 s; average linear electron density:  $(1-1.4)\times 10^{13} \text{ cm}^{-3}$ ; peripheral electron density:  $(2-4)\times 10^{12} \text{ cm}^{-3}$ ; peripheral temperature of electron: 100–200 eV. Fig.10 shows the SEM micrographs of SiC/C FGM before and after plasma irradiation. After plasma irradiation, less evident characteristics of plasma sputtering damage appears in the specimen, as shown in Fig. 8(a) and (b). According to the results of EDS experiment, no distinct change of crystal structure and increasing of crystal lattice defects were found in XRD pattern of the specimen. The results of physical sputtering indicated that the hot pressed SiC/C FGM combine the excellent erosion resistance of SiC with high thermal shock of graphite, and it is an important candidate material employed for fusion technology in the future.**



(a) before plasma irradiation

(b) after plasma irradiation

Fig. 8. SEM micrographs of SiC/C FGM (a) before and (b) after plasma irradiation.

**XRD and SEM were employed to analyze the irradiated samples. Fig. 9(a) shows the morphologies of irradiated SiC/Cu FGM sample with 80 vol.% SiC on the surface, it is conspicuous that the sample surface was seriously damaged, almost smashed, and the melting of copper was displayed (the globule size). Fig. 9(b) is the morphology of irradiated SiC/Cu FGM (P=1), in which surface contains pure ceramics, only slight cracks were found, which indicates much better sputtering-resistant property than that cermet surface of SiC/Cu FGM. XRD results shows no distinct change of crystal structure of SiC, while small increase in peak width in graphite SMF800 specimen, indicating change of crystal structure and increase of crystal lattice defects; besides, after plasma irradiation, evident characteristics of plasma sputtering damage is noticed in graphite SMF800.**

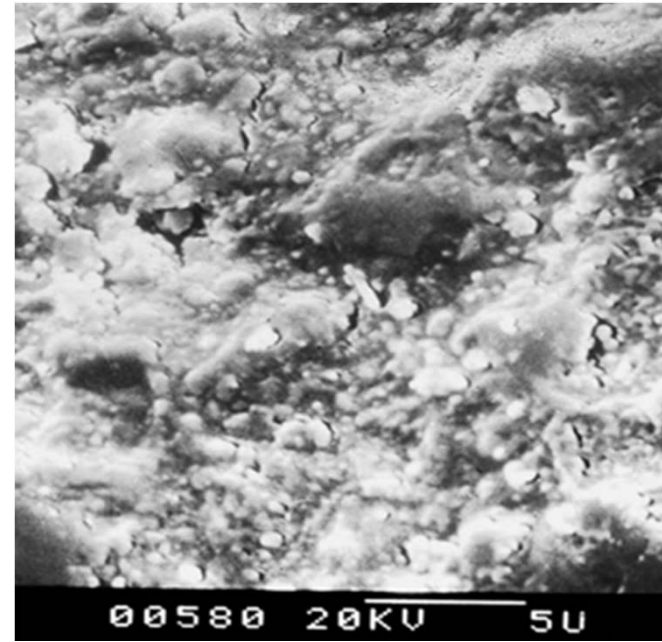
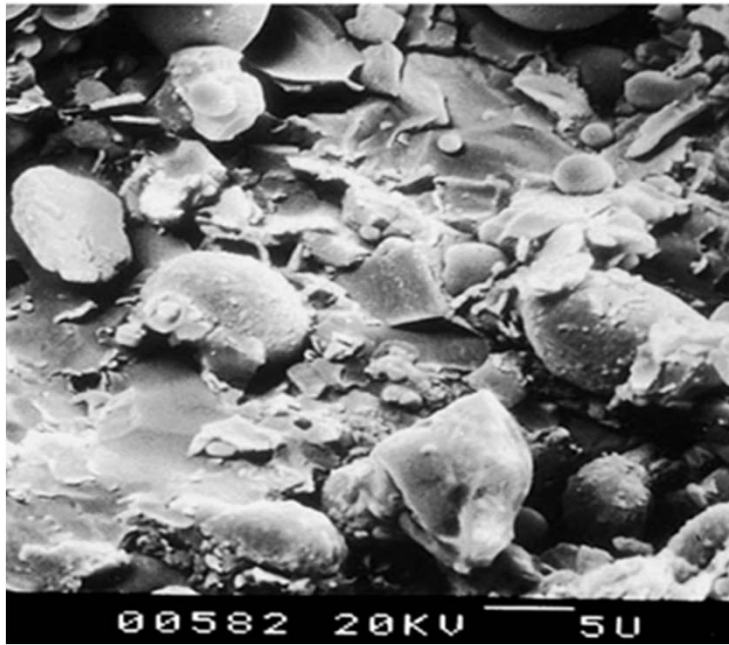
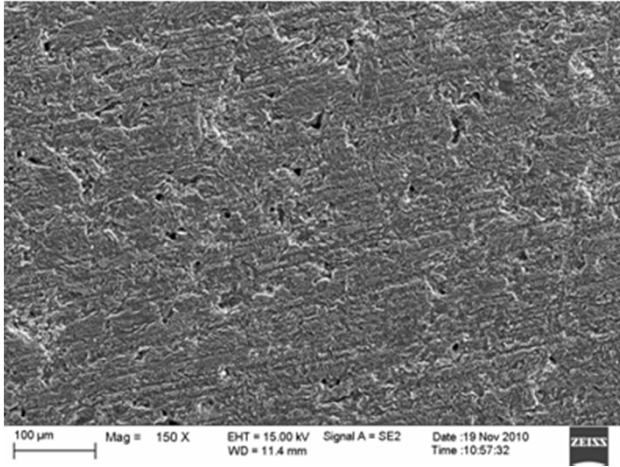


Fig. 9(a) Morphology of 80 vol.% SiC-contained surface of SiC/Cu FGM after in situ plasma irradiation. (b). Morphology of SiC/Cu FGM surface after in situ plasma irradiation.

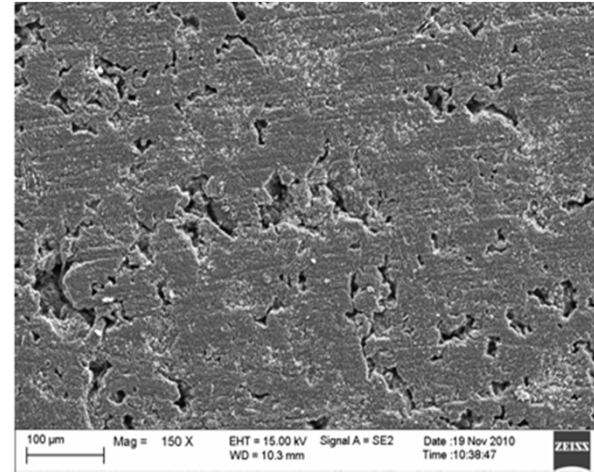
### **3.4. Helium implantation**

#### **3.4.1 with 100keV and helium ions $10^{17}/\text{cm}^2$**

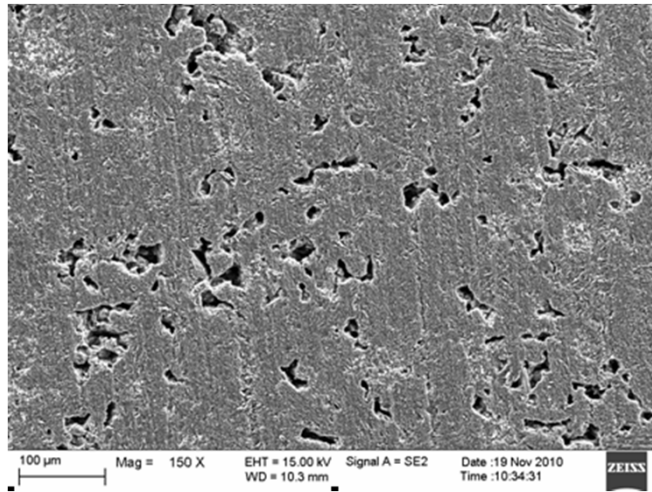
**Fig. 10, Fig. 11 and Fig.12 show the morphology of C and SiC before and after helium implantation with the energy of helium ions is  $10^{17}/\text{cm}^2$ , 100keV at room temperature and 700 °C respectively. The surface of C appears some large voids with 10~20 $\mu\text{m}$  The surface of C appears some large voids with 10~20 $\mu\text{m}$  and some voids with 5~ $\mu\text{m}$  after helium implantation. There are some small cracks and few fragments on the surface of C after helium implantation at room temperature. The surface of SiC shows much smaller changes after He implantation under the same implantation conditions. It looks like that some original small defects on the surface of the specimen before implantation enlarged to elliptical microvoids with ~2 $\mu\text{m}$ ×5 $\mu\text{m}$  and bubbles with  $\varnothing$ 1~2  $\mu\text{m}$ , while individual original voids of 1-2  $\mu\text{m}$  developed to large voids of  $\varnothing$ 2-5 $\mu\text{m}$ ×10-15 $\mu\text{m}$ , as shown in micrograph of high magnification of 3000×, which is significantly different from that of C under same condition of helium implantation. The surface of SiC shows some microvoids with 1~2  $\mu\text{m}$ . The values nano-hardness of SiC before and after helium implantation at room temperature and at 700C are 37.34, 9.5, and 29.8 GPa respectively. It shows that the value of nano hardness of SiC decreases after helium implantation.**



(a) C before helium implantation

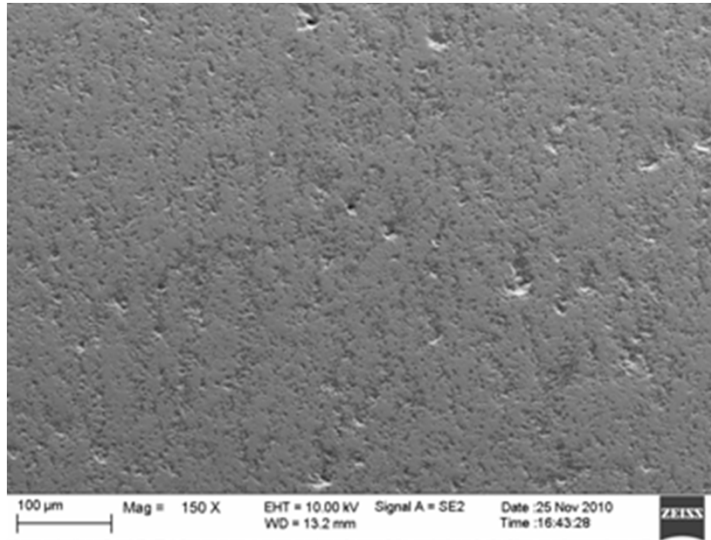


(c) C after helium implantation  
RT 100keV  $5 \times 10^{17}$  150X

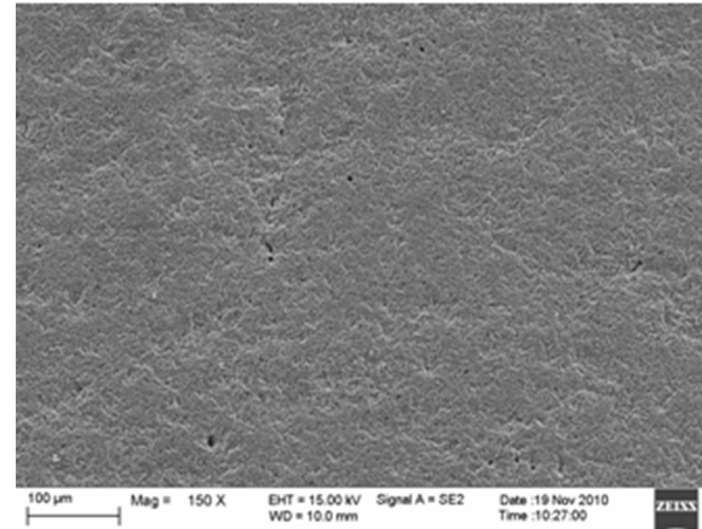


(b) C after helium implantation  
700°C 100keV  $10^{17}$  150X

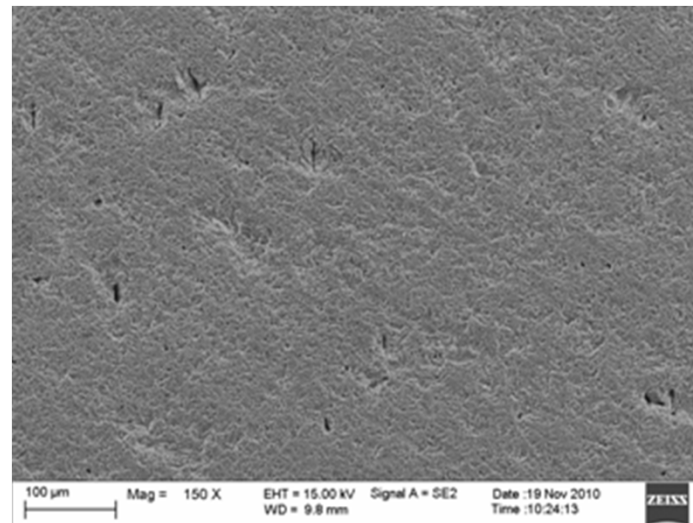
Fig. 10 Morphology of the C before and after helium implantation



(a) SiC before helium implantation

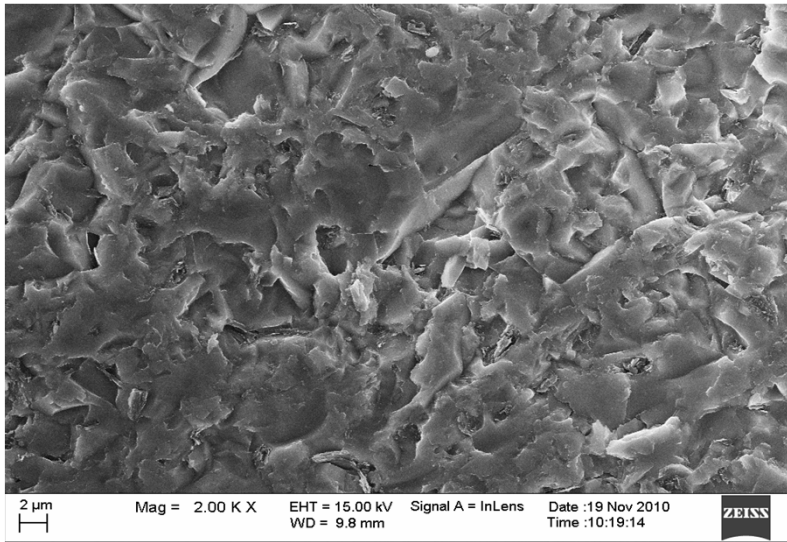


(c) SiC after helium implantation  
RT 100keV  $5 \times 10^{17}$  150X

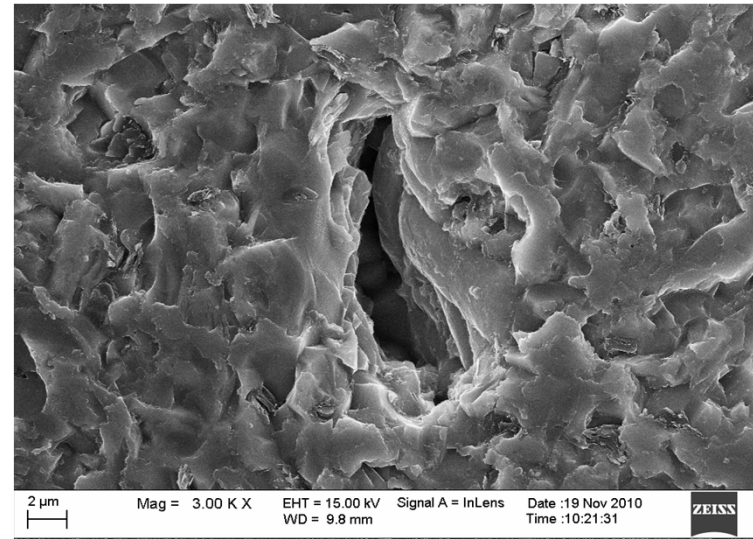


(b) SiC after helium implantation 700°C 100keV  $10^{17}$  150X

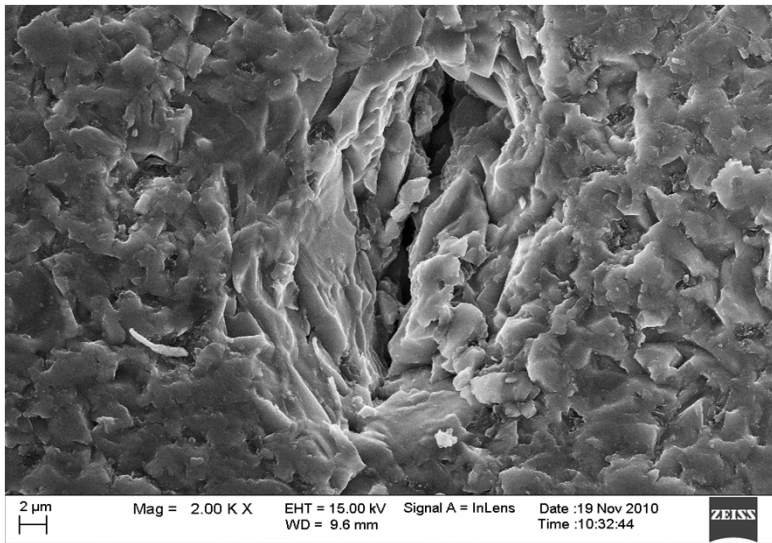
Fig. 11 Morphology of the SiC before and after helium implantation



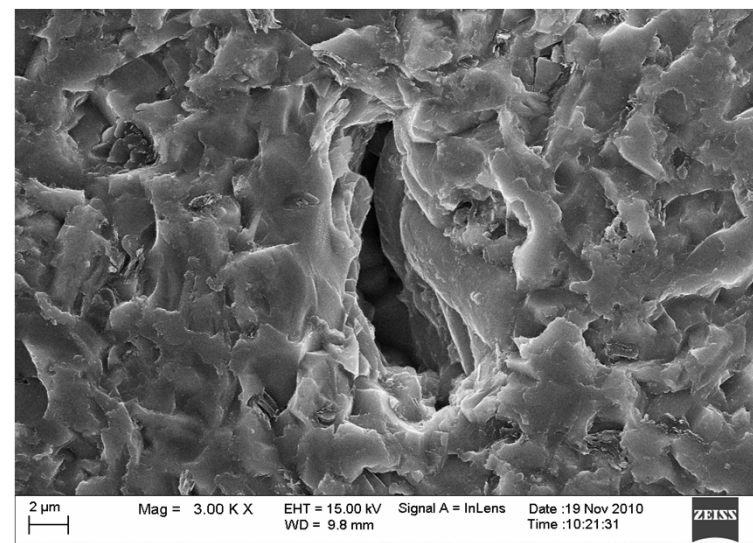
( a ) SiC RT original 2000X



( b ) SiC 700°C 100kev 10<sup>17</sup> 3000X



( c ) SiC RT 100kev 5x10<sup>17</sup> 2000X



( d ) SiC 700°C 100kev 10<sup>17</sup> 3000X

Fig.12 Morphology of the SiC before and after helium implantation

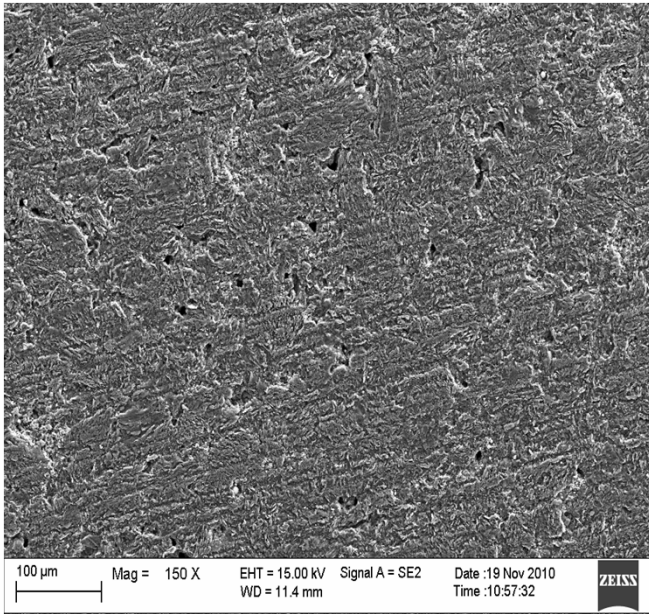
### **3.4. Helium implantation**

#### **3.4.2 with 20keV and helium ions $2 \times 10^{17}/\text{cm}^2$**

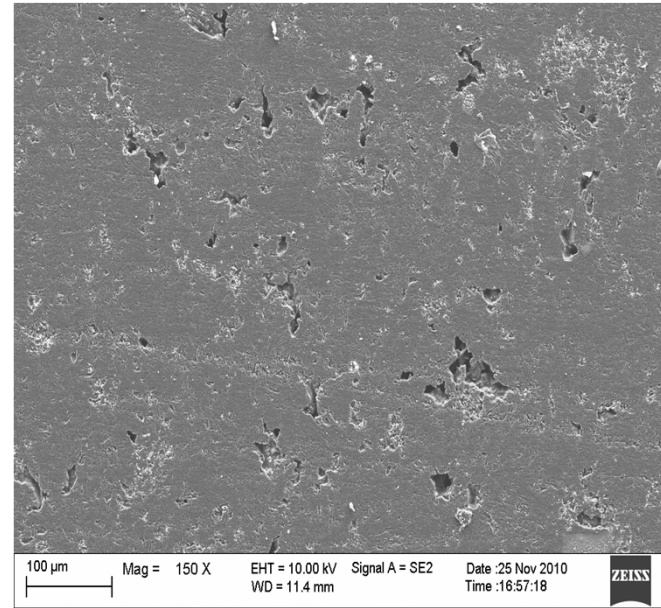
As the Fig13, Fig14, Fig15 and Fig16 show, significant difference between C and SiC after He implantation with 20keV and fluence of  $2 \times 10^{17}/\text{cm}^2$  at room temperature. Serious deterioration in microstructure and very large voids with dimensions of 6-50 $\mu\text{m}$  formed in C, while only small voids and bubbles with dimensions of 1-2 $\mu\text{m}$  homogeneously distributed in SiC, which do not change in dimension with increasing temperature.

In comparison with specimens implanted with He ions of 100keV, a series of small bubbles distributed in SiC matrix are in contrast to few large, irregular voids which might be attributed to the pores or defects existing in the original specimens before the He implantation.

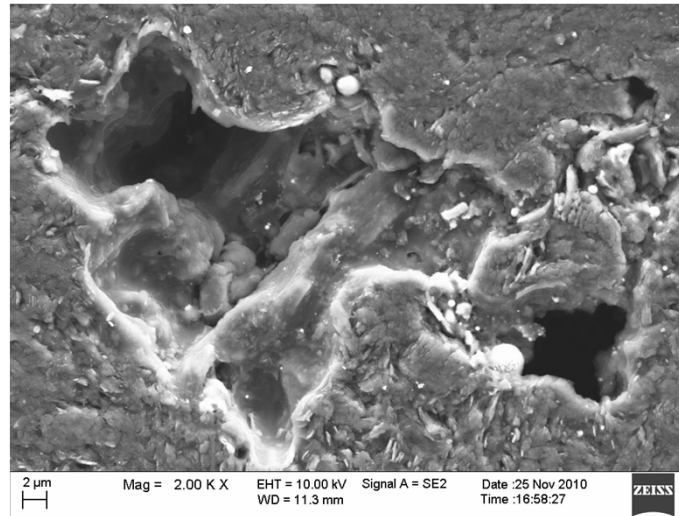
In general, no matter 20keV or 100keV used in implantation, the damages occurred in SiC are much more less than those occurred in C matrix.



(a) C before helium implantation 150X

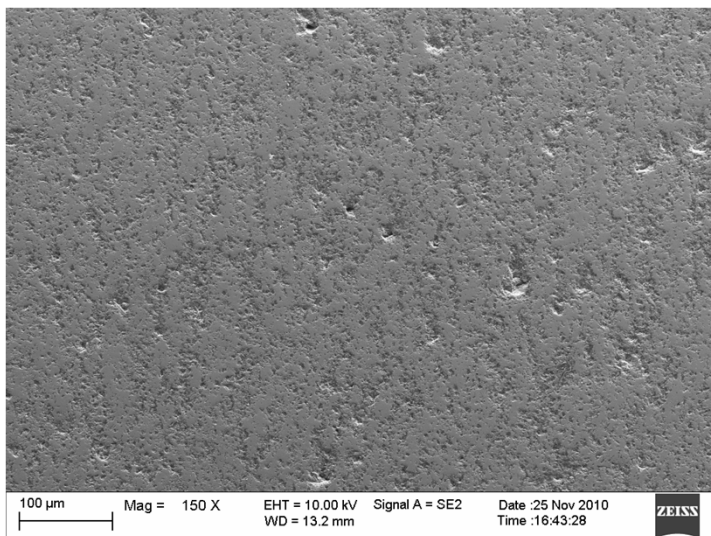


(b) C after helium implantation  
RT 20keV  $2 \times 10^{17}$  150X

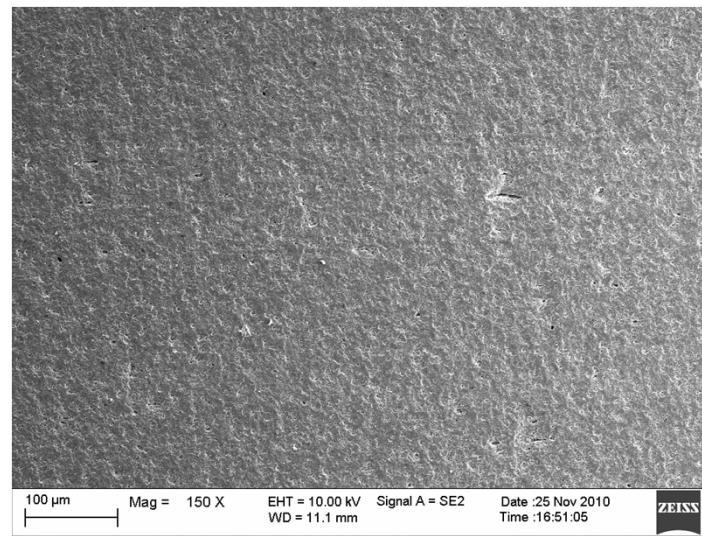


(c) C after helium implantation RT 20keV  $2 \times 10^{17}$  2000X

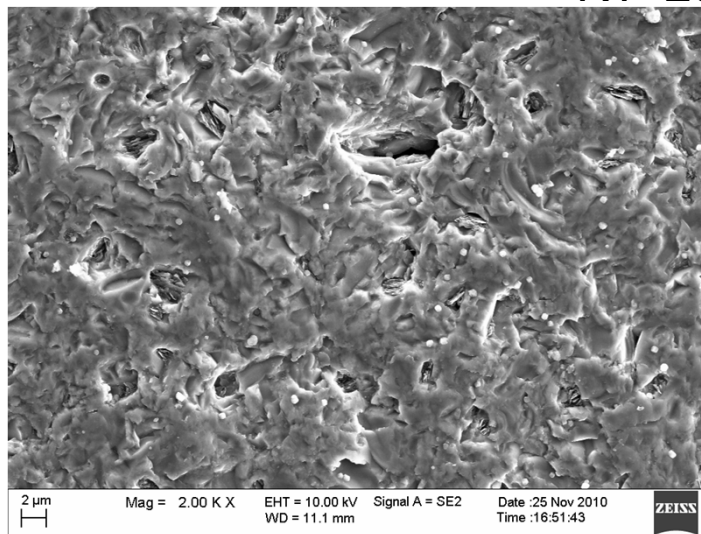
Fig. 13 Morphology of the C before and after helium implantation



(a) SiC before helium implantation 150X

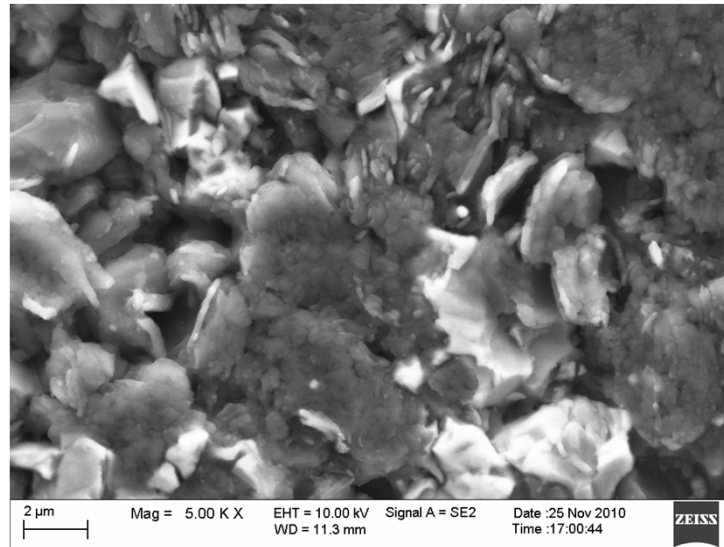


(b) SiC after helium implantation  
RT 20keV  $2 \times 10^{17}$  150X

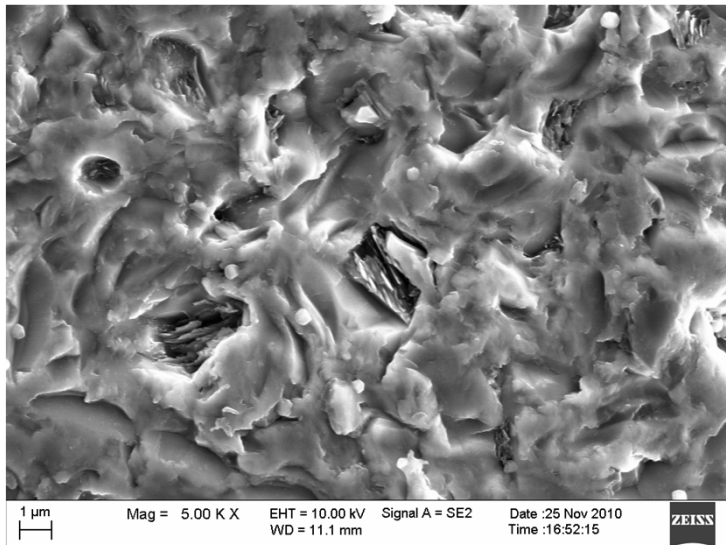


(c) SiC after helium implantation RT 20keV  $2 \times 10^{17}$  2000X

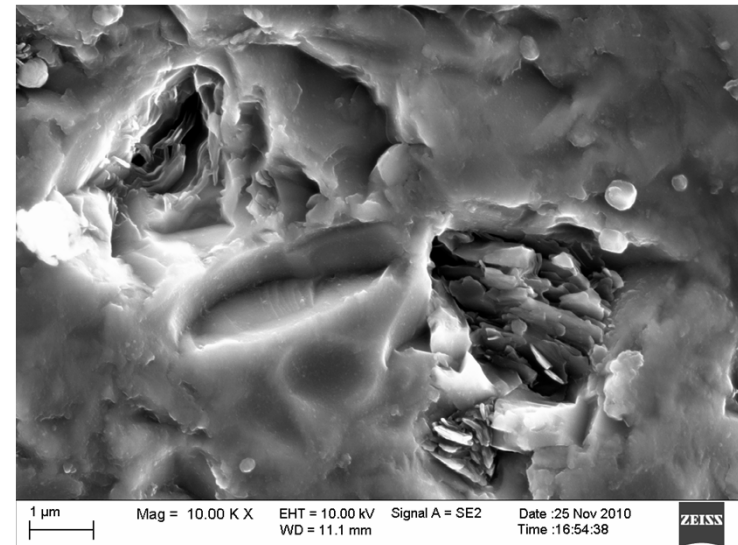
Fig. 14 Morphology of the SiC before and after helium implantation



(a) C after helium implantation RT  $2 \times 10^{17}$  5000X

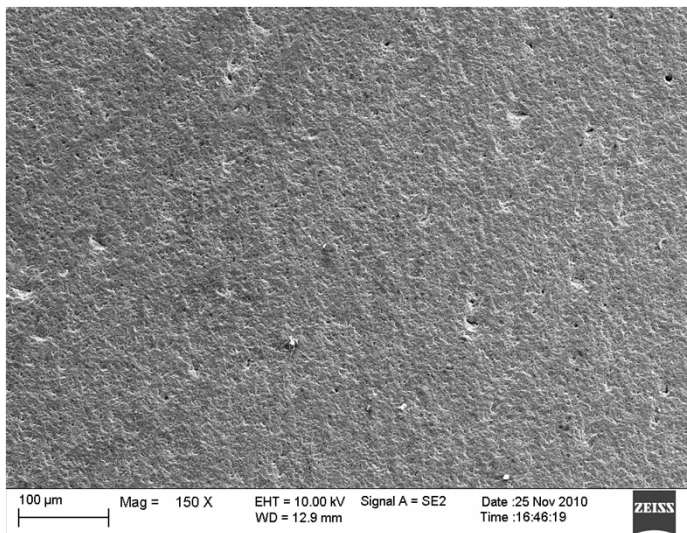


(b) SiC after helium implantation  
RT  $2 \times 10^{17}$  5000X

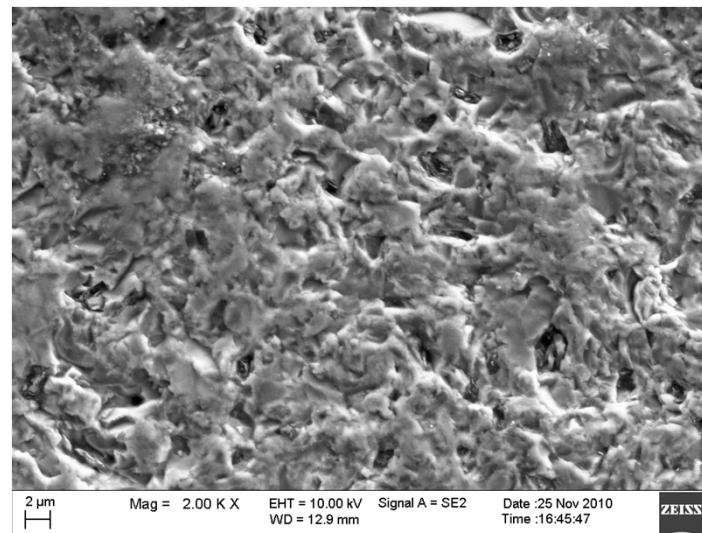


(c) SiC after helium implantation  
RT  $2 \times 10^{17}$  10000X

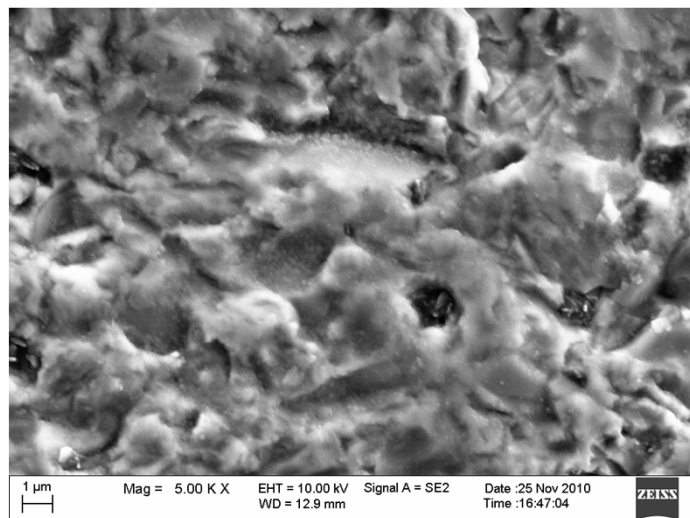
Fig. 15 Morphology of the C and SiC after helium implantation



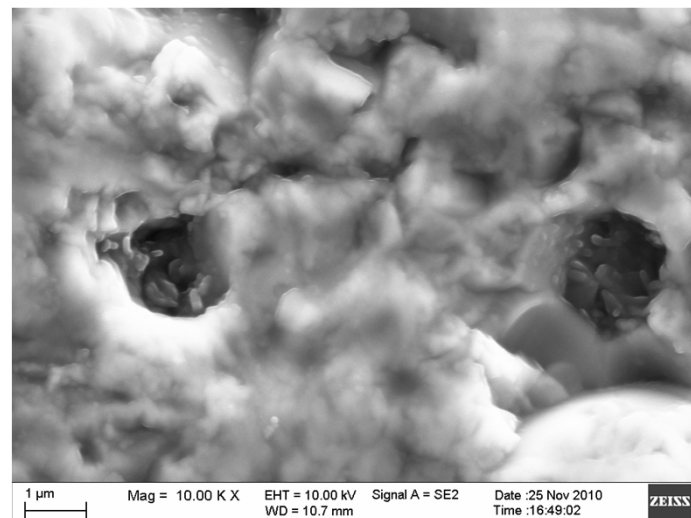
(a) SiC after helium implantation  
600°C 20keV  $2 \times 10^{17}$  150X



(b) SiC after helium implantation  
600°C 20keV  $2 \times 10^{17}$  2000X



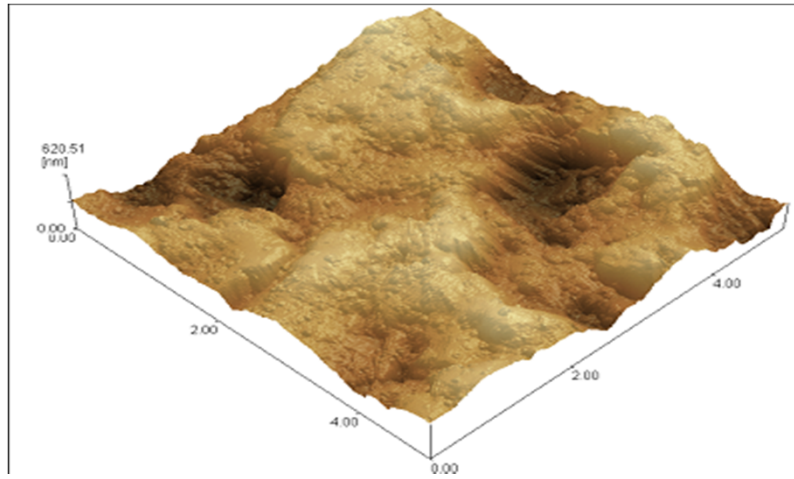
(c) SiC after helium implantation  
600°C 20keV  $2 \times 10^{17}$  5000X



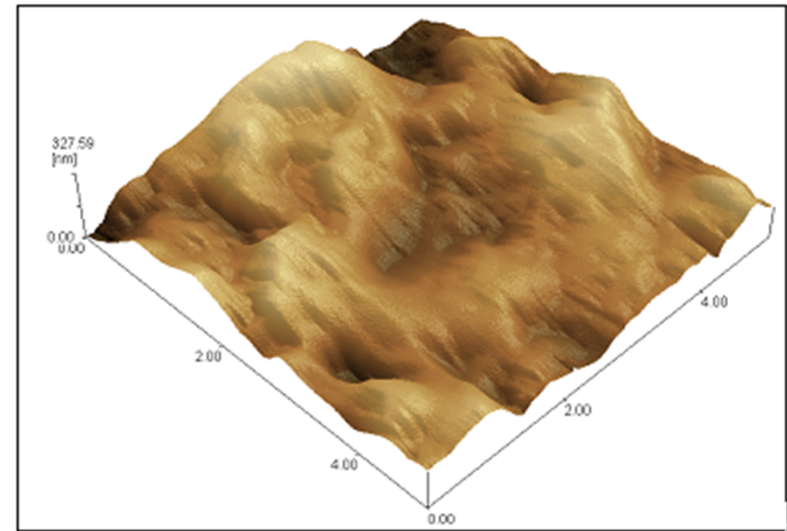
(d) SiC after helium implantation  
600°C 20keV  $2 \times 10^{17}$  10000X

Fig. 16 Morphology of the SiC after helium implantation with high temperature

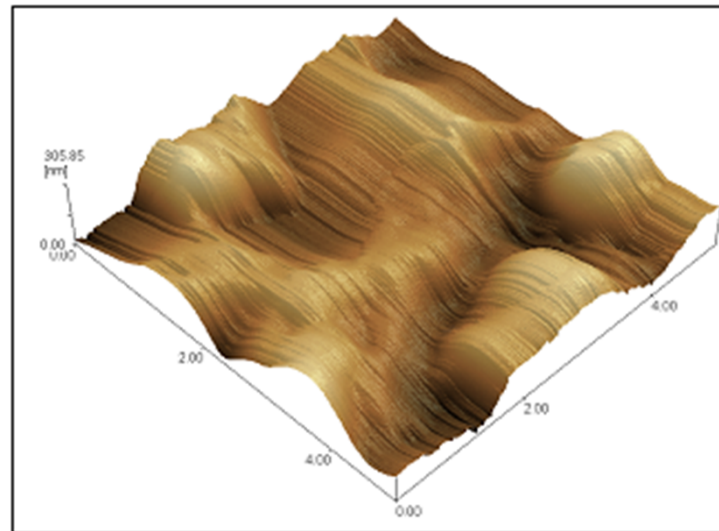
**Fig. 17 and shows the morphology of C and SiC before and after helium implantation with the energy of helium ion is  $2 \times 10^{17}/\text{cm}^2$ , 20 keV at room temperature and 600 °C, respectively in accelerator in the School of Physics and Technology of Wuhan University. It is indicated that the arithmetic mean roughness (Ra) decreases. However, the influence of temperature on the value of Ra is not significant. The surface of SiC show remarkable hollow after helium ion implantation at room and 600 °C.**



(a) Before He + implantation



(b) He + implantation at room temperature



(c) He + implantation at 600 °C

Fig. 17 the AFM imaging before and after He + implantation

## 4. Conclusion

The design, fabrication and evaluation of plasma-relevant characteristics of SiC/C and SiC/Cu FGM were Studied. SiC/C and SiC/Cu FGMs were successfully fabricated by powder stacking-hot pressing and RSUHP respectively. Less evident characteristics of plasma sputtering damage appearing in SiC/C FGM and SiC/Cu FGM after plasma irradiation indicates that SiC/C FGM and SiC/Cu FGM combines the advantages of high hot shock resistance and high heat conductivity of graphite with the advantages of high plasma-erosion resistance of SiC. The chemical sputtering of SiC/Cu FGM and SiC/Cu is one order lower than that of nuclear graphite SMF800, and the thermal desorption ratio is about 10% of that graphite. The surface of SiC/Cu FGM presents slight damage after Tokamak in situ plasma irradiation after 66 times discharges. The preliminary results show that the effect of helium implantation on SiC was less than that of helium implantation on graphite. In comparison with graphite, SiC/C FGM and SiC/Cu FGM is much more perspective to be the first wall materials for the future fusion facilities and reactors.

# **Acknowledgments**

**The authors would like to express their thanks for the International Thermonuclear Experimental Reactor (ITER) Project of China under grant No. 2010GB109000 and National Natural Science Foundation of China (No.10775108)**

**Thank you for your  
attention !**

**Institute of Nuclear Materials (INM)  
University of Science and Technology Beijing (USTB), China  
*ccge@mater.ustb.edu.cn*  
*TEL:+86-10-6233 4951***